Operation of Solid Oxide Fuel Cell Anodes with Practical Hydrocarbon Fuels

Final Report

Report Period Start Date: 10/01/2002

Report Period End Date: 09/30/2003

Principal Authors: Scott A. Barnett, Jiang Liu, Yuanbo Lin

Report Issue Date: July 30, 2004

DOE Award Number: DE-FC26-02NT41577

Submitting Organization:
Northwestern University
613 Clark Street
Evanston, IL 60208

Disclaimer

Abstract

This work was carried out to achieve a better understanding of how SOFC anodes work with real fuels. The motivation was to improve the fuel flexibility of SOFC anodes, thereby allowing simplification and cost reduction of SOFC power plants. The work was based on prior results indicating that Ni-YSZ anode-supported SOFCs can be operated directly on methane and natural gas, while SOFCs with novel anode compositions can work with higher hydrocarbons. While these results were promising, more work was clearly needed to establish the feasibility of these direct-hydrocarbon SOFCs. Basic information on hydrocarbon-anode reactions should be broadly useful because reformate fuel gas can contain residual hydrocarbons, especially methane.

In the Phase I project, we have studied the reaction mechanisms of various hydrocarbons – including methane, natural gas, and higher hydrocarbons – on two kinds of Ni-containing anodes: conventional Ni-YSZ anodes and a novel ceramic-based anode composition that avoid problems with coking. The effect of sulfur impurities was also studied. The program was aimed both at achieving an understanding of the interactions between real fuels and SOFC anodes, and providing enough information to establish the feasibility of operating SOFC stacks directly on hydrocarbon fuels. A combination of techniques was used to provide insight into the hydrocarbon reactions at these anodes during SOFC operation. Differentially-pumped mass spectrometry was be used for product-gas analysis both with and without cell operation. Impedance spectroscopy was used in order to understand electrochemical rate-limiting steps. Open-circuit voltages measurements under a range of conditions was used to help determine anode electrochemical reactions. Life tests over a wide range of conditions were used to establish the conditions for stable operation of anode-supported SOFC stacks directly on methane. Redox cycling was carried out on ceramic-based anodes. Tests on sulfur tolerance of Ni-YSZ anodes were carried out.

Table of Contents

I. Introduction

Fuel cell power plants have been successfully demonstrated many times, but the high cost of these systems has prevented commercialization. One of the key factors that contributes to this high cost is a lack of fuel flexibility. Fuel cells generally operate only on hydrogen, which is neither readily available nor easily stored. Ideally, fuel cells should be able to utilize a range of conventional hydrocarbon fuels, ranging from natural gas to propane to gasoline. To utilize hydrocarbons, fuel cell power plants usually employ fuel reforming, which convert fuels into hydrogen that can be used directly. Reforming and exhaust-gas recirculation (which provides the steam for reforming) leads to additional plant complexity and volume, increasing cost. Real fuels also contain sulfur contaminants that typically poison fuel cell anodes, decreasing performance. Thus, adsorbents must be used to remove the sulfur and the adsorbent materials must be changed or regenerated after they become saturated. Based on the above arguments, fuel cell system cost could be substantially reduced if the fuel cells themselves could operate directly on real fuels.

Recent reports have described SOFC operation directly on methane and natural gas. These results have challenged traditional views that large amounts of steam are required to prevent carbon deposition on Ni-containing anodes. Heavier hydrocarbons such as propane, butane, and even gasoline have been used directly in SOFCs[1,2] although it was necessary in this case to utilize alternate anode compositions: replacing the Ni with either Cu or a conducting ceramic. Prior to this study, there had been little attempt to understand the mechanisms whereby direct-hydrocarbon SOFCs operate.

In the Phase I project, we have studied the reaction mechanisms of hydrocarbons on two kinds of Ni-containing anodes: conventional Ni-based anodes and ceramic-based anodes. The effect of sulfur impurities and of redox cycling was also considered. The program was aimed

both at achieving an understanding of the interactions between real fuels and SOFC anodes, and at providing information required to operate SOFCs directly on hydrocarbon fuels. In particular, we have carried out detailed studies of the operation of Ni-YSZ anodes in methane-containing fuels, including cell tests, impedance spectroscopy, mass spectrometric studies of anode exhaust gas, studies of open circuit voltages, studies of the addition of H_2S to the fuel, lifetime studies designed to determine useful direct-methane operating conditions. In addition, new ceramic-based anodes have been developed that provide good performance without coking with a range of hydrocarbon fuels and are also extremely tolerant of redox cycling.

II. Executive Summary

A broad study of the operation of Ni-YSZ anode supported SOFCs directly on methane has been carried out. While many experiments remain to be done, the results are beginning to provide a clearer picture of how these cells operate. Furthermore, they have made it clear that there is a range of conditions where SOFCs can be successfully and stably operated on methane. In addition, studies of ceramic-based anodes have confirmed key advantages of these materials, including ability to work with a range of hydrocarbon fuels and good performance under redox cycling. Nonetheless, considerable work remains to be done to understand the operation of these anodes, and to improve power densities to viable levels. The following are the main conclusions of this Phase I study.

(1) Improvements in cell fabrication have allowed improvements in SOFC performance with methane fuel. Power densities as high as 0.45 W/cm^2 at 700^{o}C and 1.1 W/cm^2 at 800^{o}C have been achieved. It is clear that further improvements are possible.

(2) Open circuit voltages approaching 1.2 V are one of the reasons for the good performance in methane. Good fits to the OCV data for various fuel compositions were

obtained based on equilibrium calculations in most cases. One exception was for CH_4-CO_2-H_2O mixtures at temperatures below 750^oC, where the OCV value suggested that the fuel had not equilibrated.

(3) EIS measurements were carried out primarily on SOFCs, because attempts to do measurements on symmetric anode samples did not yield reasonable results. The SOFC results showed that the cathode polarization dominated only at very low current density. With increasing current, the cathode polarization decreased rapidly to a saturation value, whereas the anode polarization increased continuously with increasing current. The anode polarization was substantially larger for methane than for hydrogen. These results indicate that gas diffusion in the anode support played an important role in determining cell performance; this suggests that, in general, SOFC performance will be strongly dependent on anode parameters including thickness, porosity, and tortuosity. For ceramic-based anodes, the anode polarization was substantially larger in propane than for hydrogen.

(4) Mass spectrometer measurements showed that the expected reaction products – H_2, H_2O, CO, and CO_2 – all increased with increasing cell current density. The dominant products at 800^oC were H_2 and CO, in agreement with thermodynamic predictions. However, the thermodynamic predictions could not directly explain the lack of coking during direct methane operation.

(5) The nature of the key anode reaction(s) remains unclear at this stage. While there is good reason to think that substantial hydrogen is produced within the Ni-YSZ anode, the OCV values observed experimentally cannot be explained by a hydrogen oxidation

reaction. More work, particularly detailed modeling of diffusion and reaction processes within the anode, is needed.

(6) We have mapped out the stability region for direct methane operation. The key features are as follows. At lower temperatures, $\leq 700^{o}C$, stable operation without coking occurs over a wide range of current densities. At higher temperatures, on the other hand, increasingly large currents are required to avoid coking and cell failure. Fuel gases containing lesser amounts of methane appear to have a much wider stability range. Thus, direct-methane SOFC stacks would be best operated at lower temperatures. Even a minimal partial reforming of the methane, prior to introduction to the stack, will substantially improve stability.

(7) Degradation of cell performance was observed for H_2S-contamined H_2 fuel at $800^{o}C$, but surprisingly the degradation was negligible at $700^{o}C$. Further work is needed to explore these effects.

(8) Further experiments have been carried out on ceramic-based anodes. Cells tests with these anodes have shown good fuel flexibility, including hydrogen, methane, ethane, propane, and butane. Excellent cell stability, particularly in redox cycling with hydrogen-air and propane-air, has been demonstrated. Increased power densities are required, however.

III. Experimental

A large number of Ni-YSZ anode-supported fuel cells have been prepared to study cell stability in hydrocarbon fuels. Ni-YSZ anode supports were made by mixing NiO (Baker) and 8-YSZ (Tosoh), in a weight ratio of 1:1, and ball milling in methanol for about 20 hours. 9wt% of starch was then added to the mixture and the ball milling was continued for another two hours. The milled powder mixture was dried and pressed into pellets with diameter of 19 mm and thickness of about 1.0 mm. The pellets were pre-fired at 1000°C for 4 hours. An YSZ electrolyte layer was coated on the anode support by centrifugal casting[3] and then was co-sintered at 1400°C for 4 hours. A $La_{0.4}Sr_{0.4}Fe_{0.2}Co_{0.8}O_3$ (LSCF) (Praxair) (50wt%)-GDC (50wt%) cathode was applied on the YSZ electrolyte and fired at 950°C for 3 hours. On the top of LDCF-GDC cathode layer, another pure LSCF layer was applied and co-sintered at 950°C for 3 hours.

GDC-supported-electrolyte SOFCs have been prepared for studies of $LaCrO_3$-based anodes. GDC pellets ≈ 0.5mm thick were produced by uniaxial pressing. Anodes were applied and then the anode/electrolyte co-sintered at 1500°C for 6 hrs. The anodes consisted of 48 vol% $(La,Sr)(Cr,V)O_3$ (LSCV) powder, synthesized by the solid-state reaction method, 48 vol% GDC (NexTech) with a 50 nm average particle size, and 4% NiO (Nanophase), with a 16 nm average particle size. X-ray diffraction measurements on the anodes showed distinct LSCM, GDC, and NiO peaks. LSCF cathodes were then applied as described above. Since the power density of cells with these thick electrolytes is severely limited, as are the practical applications of such cells, we have made attempts to prepare anode-supported SOFCs on $LaCrO_3$-based anodes. These were unsuccessful due to the difficulty of sintering the chromite material. Our focus thus shifted to $(Sr_{0.7}La_{0.3})TiO_3$ (SLT) supports. Porous SLT supports with dense YSZ electrolytes have been successfully prepared by centrifuge coating SLT pellets and co-sintering at 1400^oC.

Symmetrical samples for anode impedance studies have also been prepared. The first type consists of bulk YSZ electrolytes with identical Ni-YSZ anodes on both sides. Second, we attempted to make samples by sintering together two YSZ/NiO-YSZ bi-layers, placed with the YSZ faces in contact. This was found to not give good contact between the YSZ layers. We have also prepared impedance samples with single-crystal YSZ electrolytes in order to avoid grain-boundary effects; however, we still see substantially larger impedance arcs in these symmetrical samples than in actual cells. The reason for this problem is not clear, but as a practical measure in Phase I, we focused on measurements of cells versus symmetrical anode samples.

Basic characterization using SEM and energy-dispersive x-ray analysis was carried out using a Hitachi 3500 microscope. X-ray diffractions measurements were done with a standard powder diffractometer.

SOFC tests were carried out from 500 to 800C with air at the cathode and a variety of fuel gases. For Ni-YSZ anode cells, the anodes were first reduced in humidified hydrogen (~3%H_2O) by keeping the cell at 700 to 800C for several hours. The I-V curves and electrochemical impedance spectra (EIS) were obtained using an IM6 Electrochemical Workstation (ZAHNER, Germany). The frequency range for the impedance measurement was 0.1Hz to 100KHz. Anode exhaust gas was sampled during cell operation using a differentially-pumped mass spectrometer.

IV. Results and Discussion

1. Basic SOFC Testing

Ni-YSZ Anodes

Figure 1 shows typical voltage and power density vs. current density of a SOFC operated on humidified hydrogen (a) and methane (b). The maximum power density was ~1.1W/cm^2 at 800°C for both fuels. Note that operation in methane was not stable under some conditions, especially high *T* and low *J*; this is discussed in detail in section 5 below. The open circuit voltage (OCV) in methane increased with increasing temperature, opposite of the usual trend shown for hydrogen. This trend agrees reasonably well with the OCV predicted based on the equilibrium anode gas composition: this is discussed further in section 2. The I-V curves are not linear. For methane, the initial resistance is higher than for hydrogen. A similar gas diffusion limitation can be seen for both fuels at 800^{o}C. This effect was explored in more detail using impedance spectroscopy (see section 3 below).

Ceramic Anodes

Figure 2 shows typical test results for a GDC-electrolyte cell with a LSCV-GDC-Ni anode, operated in humidified propane fuel. Note that the power densities are relatively low compared with typical anode-supported cells because of the high resistance of the thick GDC electrolyte; EIS results indicated that this resistance comprised 60-70% of the overall cell resistance. Also, the OCV values for these cells were relatively low, especially for the higher temperatures, due to the mixed conductivity of the GDC electrolyte. Despite these limitations, the cell achieved maximum power densities of 120 mW/cm^2 at 650^{o}C and 150 mW/cm^2 at 750^{o}C.

Figure 3 shows test results for the same cell operated with hydrogen, methane, ethane, propane, and butane fuels at 700^{o}C. The cell operated stably for several hundred hours on a variety of fuels. The cell characteristics and power densities were similar with all the fuels – this is perhaps not surprising given that the cell performance was limited primarily by the electrolyte

(a)

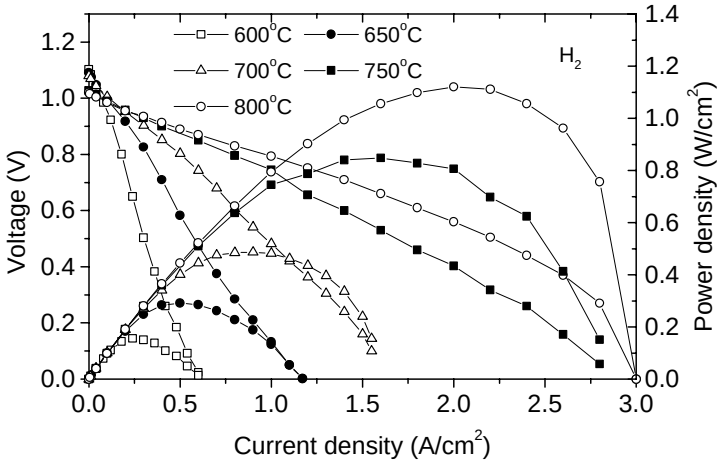

(b)

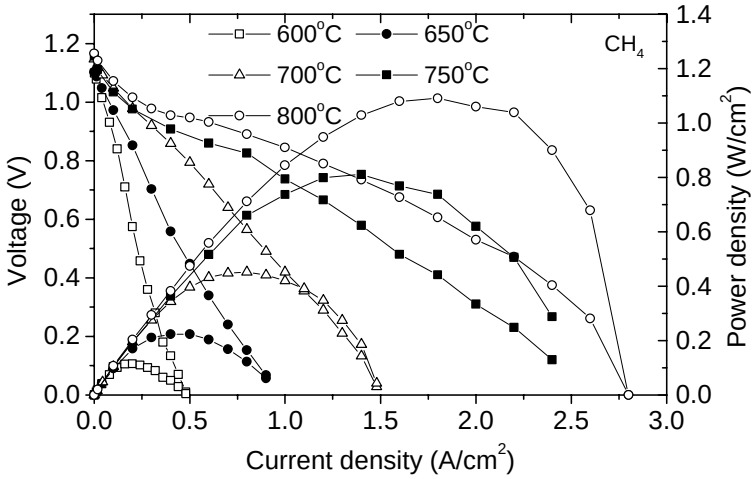

Figure 1. Voltage and power density vs. current density of a SOFC operated on humidified hydrogen (a) and methane (b).

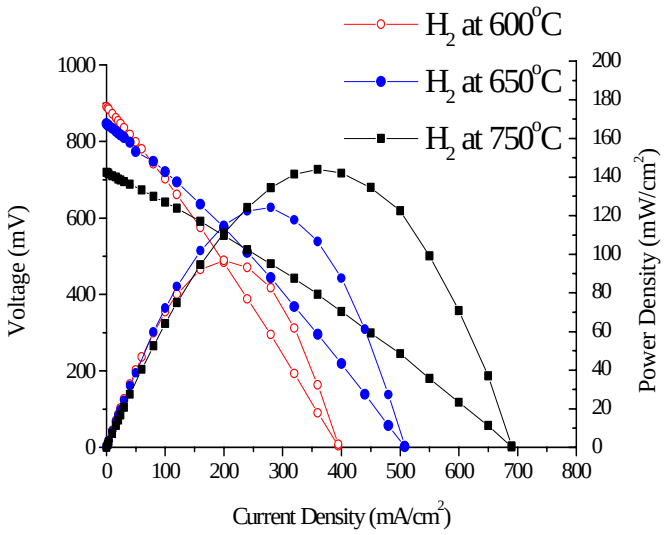

Figure 2. Voltage and power density vs. current density for a GDC-electrolyte cell with a LSCV-GDC-Ni anode, operated in humidified propane fuel.

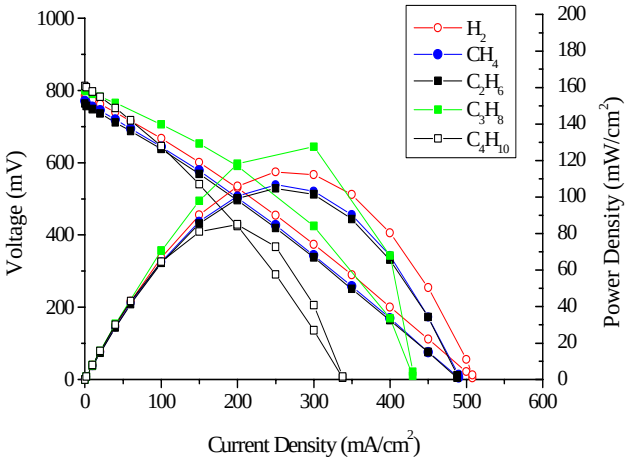

Figure 3. Voltage and power density vs. current density for a GDC-electrolyte cell with a LSCV-GDC-Ni anode operated in various fuels at 700°C.

resistance. Note that similar results have been obtained in cells with doped $SrTiO_3$-based anodes.

While these ceramic-based anodes show good promise for fuel-flexible SOFCs, it is clear that their practical application will require that they be implemented in thin-electrolyte cells where the electrolyte does not have significant electronic conductivity. We have thus begun the fabrication of anode-supported SOFCs using $(Sr,La)TiO_3$ (SLT) supports and YSZ (or Ceria/YSZ) electrolytes. While the resistance of $(Sr,La)TiO_3$ ($\approx 0.1\Omega$cm) is higher than that of Ni-YSZ, the area-specific resistance of a 1-mm-thick anode support is still only $0.01\Omega cm^2$. This approach is also interesting because the raw materials for the LST supports will be quite inexpensive. At present, anode-supported electrolytes have been successfully prepared by co-sintering, but testing has not yet been carried out.

2. Open circuit voltage measurements

As noted in Figure 1, OCV values for methane increase with increasing T. The OCV values are plotted versus T for both hydrogen and methane in Figure 4. Also shown are predicted OCV values, assuming that the humidified methane reaches equilibrium. The experimental and predicted OCV values are in good agreement, except that the experimental values are ≈ 50mV lower. This was presumably due to experimental issues, e.g. slight gas leaks in the cell test. This suggests that the fuel reached equilibrium at the anode.

As a further test to determine if the fuel gas was reaching equilibrium at the anode, CO_2 gas was added to the fuel stream. The predicted response is different depending upon whether the CO_2 does not react, reacts with other fuel components (e.g. CH_4) to produce a new equilibrium gas composition, or is the product of a specific reaction (e.g. $CH_4 + 2O_2 = CO_2 + 2H_2O$). Results of OCV measurements with CO_2 added to H_2 and CH_4 fuel gave good agreement

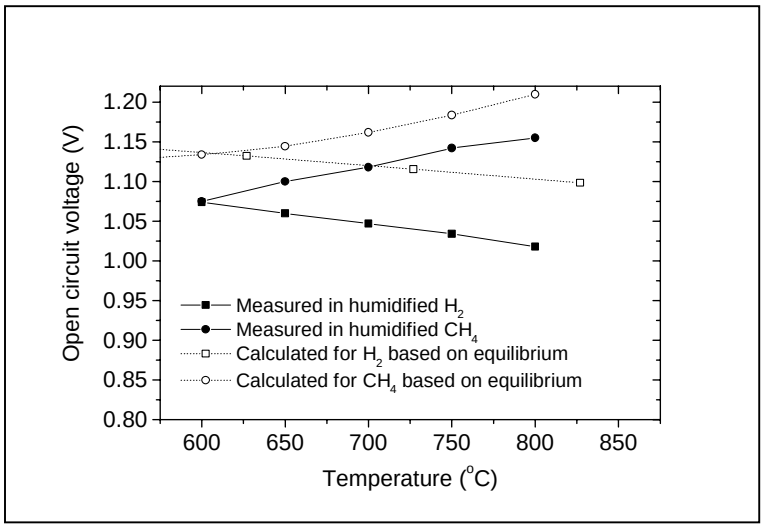

Figure 4. Open circuit voltage values versus T for both hydrogen and methane. Also shown are the values predicted by assuming that the humidified methane reaches an equilibrium composition.

with calculated equilibrium OCV values for cell temperatures >700^{o}C, suggesting that reaction kinetics are sufficient for the fuel mixture to approach equilibrium. Figure 5a shows the change in OCV with CO_2 amount added to humidified hydrogen. The OCV decreases substantially with increasing CO_2, and agrees reasonably well with the OCV calculated assuming equilibrium. Also shown is the OCV calculated assuming the CO_2 is an inert diluent, which does not agree with the data. Figure 5b shows the change in OCV with T for CH_4 with 20% CO_2 added. The equilibrium calculated OCV, also shown, follows a similar trend to that shown in Figure 4, but with a lower OCV due to the added CO_2. The experimental results agree with the prediction reasonably well for ≥750C, but the measured OCV was higher than the predicted value at lower T. This suggests that the anode was not seeing an equilibrated fuel-gas mixture. Indeed, the OCV at low T begins to approach the OCV calculated assuming CO_2 was an inert diluent (see Fig. 5b). Note that the OCV predicted assuming direct methane electrochemical oxidation yields lower OCV than the data, precluding this as a possible anode mechanism. Thus, it is dangerous to assume that the fuel gas reaches equilibrium under all conditions, especially low temperature.

3. Electrochemical Impedance Spectroscopy (EIS)

Ni-YSZ Anodes

Considerable effort was invested in Phase I to make EIS measurements on symmetrical anode samples – this measurement has the advantage of having a clear interpretation because of the symmetry of the impedance geometry. However, the symmetrical samples invariably showed polarization resistances much larger than observed in SOFCs. We have looked at the possibility that the large resistance is associated with the reverse current flow direction through one of the anodes during the symmetrical test. However, our cell measurements with current reversed (electrolysis) do not show a substantial difference in impedance with current direction.

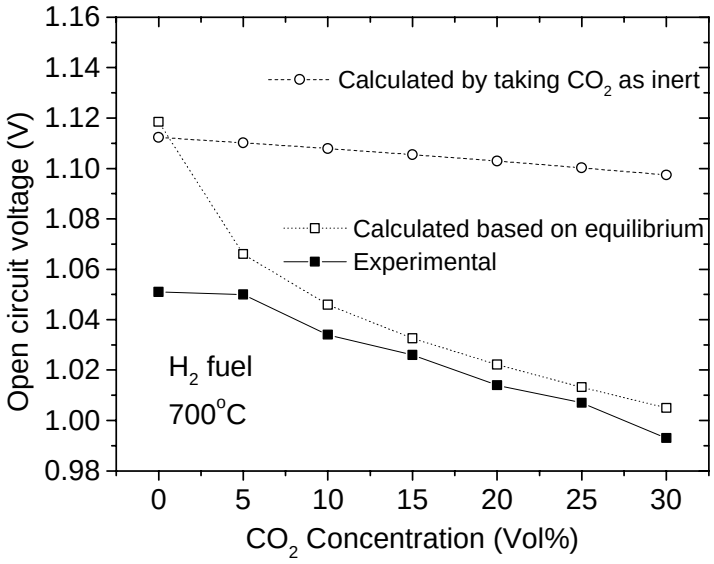

Figure 5a. OCV variation with CO_2 amount added to humidified hydrogen. Also shown for comparison are predicted OCV values assuming an equilibrium fuel and a case where the CO_2 is assumed inert.

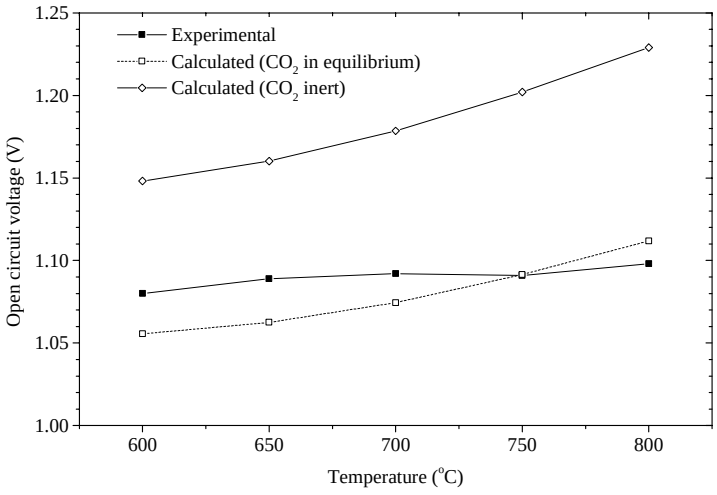

Figure 5b. OCV variation with T for humidified CH_4 with 20% CO_2 added. Also shown for comparison are the calculated OCV values assuming the fuel reaches equilibrium, and assuming the CO_2 is inert.

We have also tested impedance samples with single-crystal YSZ electrolytes, in order to eliminate any grain boundary arcs. While this did decrease the impedance, it was still very large compared with SOFCs. The reason for this discrepancy is not clear, but we abandoned this approach and focused on measurements on anode-supported cells.

Extensive EIS testing on anode-supported cells has been carried out. While the non-symmetrical nature of these samples leaves some issues regarding the exact interpretation of the EIS data, most researchers believe that realistic trends can be determined using even a relatively simple EIS interpretation. We can resolve anode and cathode arcs by switching the gas compositions on the respective sides of the cells.

Impedance spectra were taken for a SOFC operated in humidified H_2 and CH_4 at different currents at 700°C. Figure 6 shows the EIS measured at 700°C in humidified H_2 at open circuit. Note that the EIS was not measured at open circuit for methane, because the slow coking that occurred at 700°C at OCV changed the cell characteristics during the ≈ 10 min EIS measurement, creating artifacts. The first real-axis intercept is at 0.12 Ωcm^2, corresponding to the Ohmic resistance of the cell. There is an apparent double arc observed. The main portion of this arc at lower frequency did not vary with fuel gas composition, and was thereby associated with the cathode. This is in accord with many other results showing that the cathode dominates the cell polarization resistance at OCV. Fits were made to the cathode arc using the usual model for LSCF-based cathodes,[4] where the rate-determining steps are surface exchange and solid-state diffusion, yielding a Gerischer-type response given by

$$Z = R_{chem}\sqrt{\frac{1}{1 - j\omega t_{chem}}}\ , \qquad (1)$$

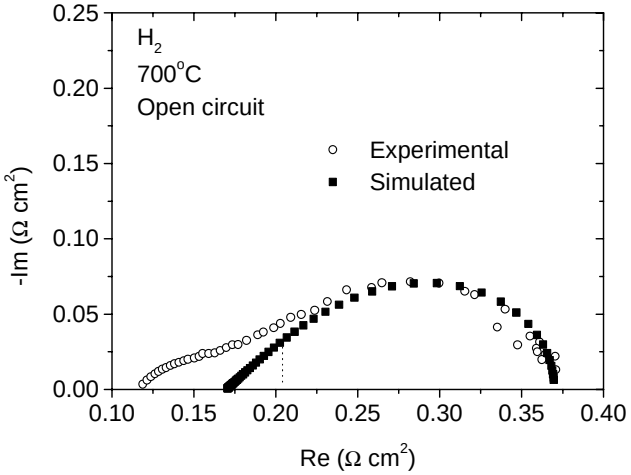

Figure 6. Nyquist plot of an electrochemical impedance spectroscopy result from an anode-supported cell measured at 700°C in humidified H_2 at open circuit. Also shown is a fit to the low-frequency arc using eq. 1.

where t_{chem} is the relaxation time related to the chemical processes of solid-state diffusion and O_2 surface exchange, and R_{chem} is the characteristic resistance describing the chemical contributions to the cathode impedance. A fit to the arc using eqn. 1, shown in Fig. 6, yielded a good fit to the low frequency portion. The high frequency portion was apparently associated with the anode process.

The character of the impedance spectra changed considerably at non-zero *J* values, as shown in Fig. 7a (hydrogen) and Fig. 7b (methane) at 700°C for $J = 400 mA/cm^2$. The higher-frequency (anode) arc has increased in size, becoming the dominant feature, while the low-frequency (cathode) arc has become smaller. The figures also show that fits to the low-frequency arc using eq. 1 are reasonably good. The fact that the arc size was the same for both fuels supports the idea that these are cathode arcs. The high frequency arc is ≈ 3 times larger for methane than for hydrogen, and the shape of the arc is different.

Figure 8 summarizes the sizes of the high- and low-frequency EIS arcs as a function of *J*. The low-frequency arcs, almost the same for H_2 and CH_4, decrease rapidly as *J* increases above 0, and then saturate, as expected for activation polarization. On the other hand, the high frequency arc increases steadily with increasing *J*, reaching a maximum at $J = 1.2\ A/cm^2$, before decreasing slightly. The decrease at high *J* is not understood at present. The same trend is observed for both fuels, but the arc is larger for methane. A polarization increase with *J* is consistent with mass transport polarization, which can be expressed as[5]

$$R(J) = R_0 + (RT/2F)\{[1/(J_{as}-J) + 1/(rJ_{as}+J)\}, \quad (2)$$

where J_{as} is the anode limiting current

$$J_{as} = 2Fp_{H2}D_{a(eff)}/RFl_a, \quad (3)$$

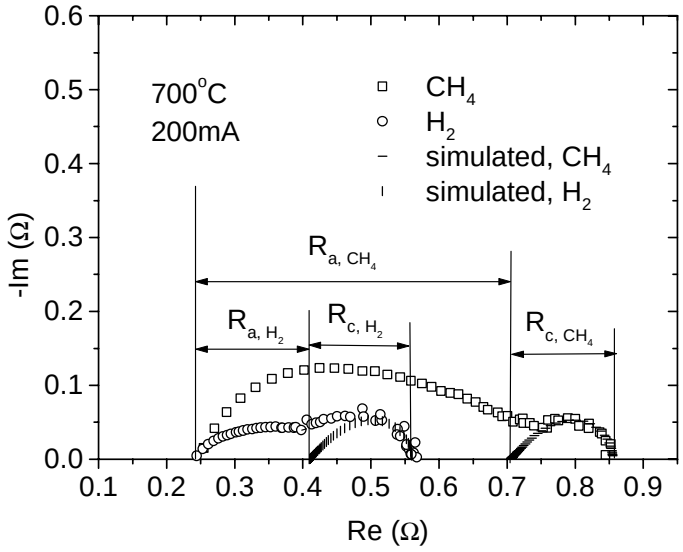

Figure 7. Electrochemical impedance spectra at 700°C for the cell shown in Fig. 6, but taken at J = 400mA/cm^2, for both hydrogen and methane. Also shown are fits to the low frequency arcs using eq. 1.

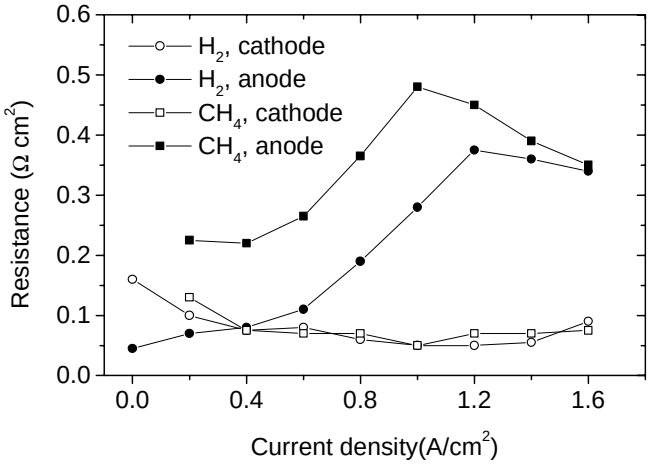

Figure 8. A plot of the real-axis intercepts for the low-frequency (cathode) and high frequency (anode) arcs as a function of cell current density.

$r = p_{H2O}/p_{H2}$, the partial pressures are the values in the gas stream, $D_{a(eff)}$ is the effective gas diffusion coefficient in the anode, l_a is the anode thickness, R is the gas constant, and F is Faraday's constant. Equation 2 provides a reasonable explanation for the increase in anode polarization with increasing *J*. The anode polarization for CH_4 also increases with increasing current, but is larger than for H_2. There is a larger *J*=0 polarization for methane, but the mass transport limitation appears to be similar for hydrogen and methane.

These results show that anode polarization became the dominant loss at higher *J* values, and that the loss was substantially larger for methane. This loss may have been related to slow kinetics for a methane oxidation or dissociation step, or possibly due to a low hydrogen concentration (assuming that the anode reaction was primarily hydrogen produced within the anode). Since mass transport plays an important role in the anode impedance, it is clear that, in general, results for anode-supported cells may vary widely for different anode supported cells depending on anode thickness, porosity, and tortuosity (the latter two determine $D_{a(eff)}$ in eq. 3).

Ceramic Anodes

Impedance measurements have been carried out on SOFCs with ceramic-based anodes, i.e. $(La,Sr)(Cr,V)O_3$ with Gd-doped Ceria and a small amount of Ni. An example is shown in Figure 9, where it is seen that there are two main impedance arcs associated with the anode for both hydrogen and propane. The anode polarization increased by ≈30% for propane relative to hydrogen, but there was relatively little change in the shape of the arcs.

4. Anode reaction products

In order to obtain a clearer picture of anode reactions with methane, mass-spectrometer measurements of the anode exhaust gas have been carried out. Figures 10a and 10b show the real-time changes in the exhaust CO_2 and H_2O as a function of *J*, during SOFC operation in

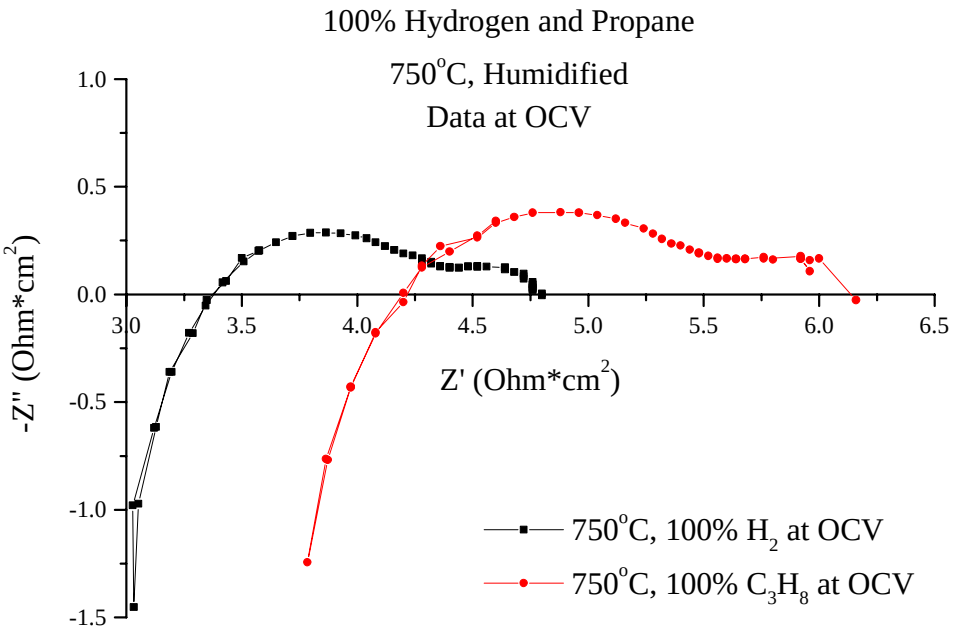

Figure 9. EIS results taken at OCV for a GDC-electrolyte cell with a LSCV-GDC-Ni anode in hydrogen or propane.

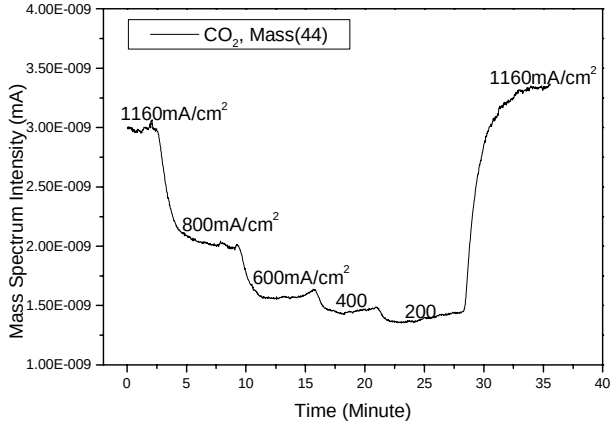

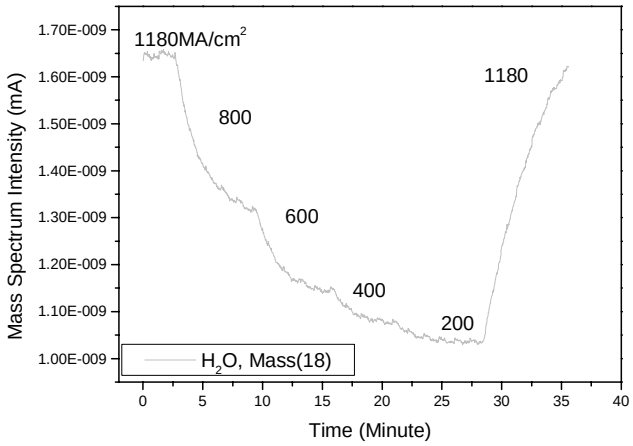

Figure 10. Real-time changes in the exhaust gas composition versus cell current density *J* during SOFC operation in humidified methane at 800°C, observed via the mass 44 (CO_2) signal (a) and mass 18 (H_2O) signal (b).

humidified methane at 800°C. The lag times for the measured partial pressures to stabilize were related to the time required for the anode gases to reach the mass spectrometer through the sampling tube and differential pumping system. The lag time for H_2O was longer, presumably due to the tendency of H_2O to adsorb on surfaces. One problem with the mass spectrometer data is the "zero blast", which causes the mass spectrometer to under-estimate the size of the hydrogen peak. Figure 11 shows the concentration changes for various products derived from the mass spectrometer data. Each of the species H_2, CO, CO_2, and H_2O increased with increasing *J*, but the increases in H_2 and CO were substantially larger.

Figure 12 shows results of thermodynamic calculations of the equilibrium anode gas composition assuming an input fuel composition of humidified (~3% H_2O) CH_4, and including the addition of oxygen via fuel cell operation, at 700 and 800°C. A similar calculation based on diluted dry methane feed gave similar results.[6] At low current density *J*, and hence O_2-to-CH_4 ratio χ,, the reaction products – primarily solid carbon and hydrogen – indicate methane cracking. As χ increases up to 0.5, the main change is that solid carbon is replaced by CO. That is, the dominant reaction resulting from SOFC operation was partial oxidation of C. Note that increasing χ to ≥0.5 eliminates coking. This general trend has been reported previously.[7] Finally, as χ increases above 0.5, H_2 and CO are increasingly replaced by H_2O and CO_2. The amounts of H_2O and CO_2 are generally larger at lower temperatures.

Figure 12 can be compared directly with the mass spectrometer results shown in Fig. 11, since increasing *J* is the same as increasing χ. The rapid increase in CO content and slight increases in CO_2 and H_2O in Fig. 11 agree well with Fig. 12. While the prediction does agree with the high H_2 content shown in Fig. 11, the trend is different. Overall, it is not surprising that the experimental results agreed reasonably well with thermodynamic predictions: even if the

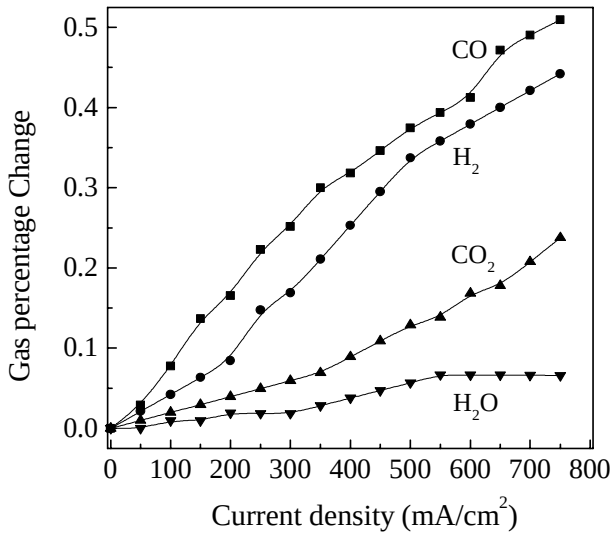

Figure 11. Changes in the concentrations of various species versus SOFC current density during operation in humidified methane at 800°C, derived from the mass spectrometer data.

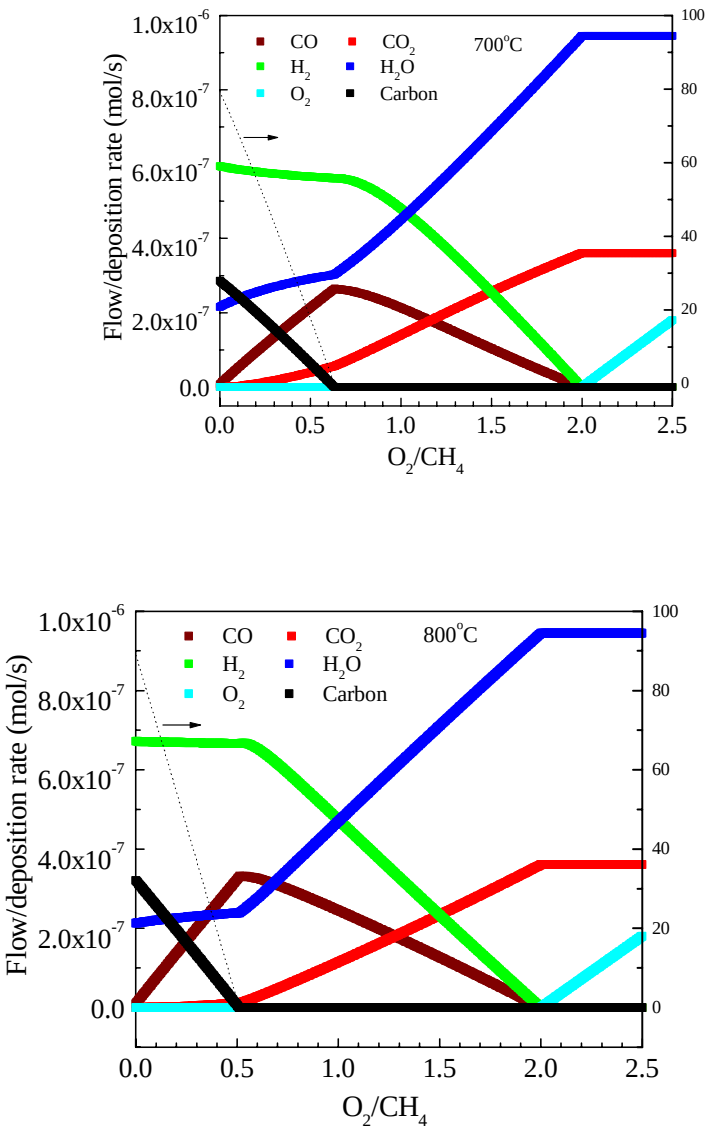

Figure 12. Thermodynamic prediction of the equilibrium anode gas composition, assuming an input fuel composition of humidified (~3% H_2O) CH_4, versus the oxygen-to-methane ratio, at 700 (a) and 800°C (b).

actual electrochemical reaction products are non-equilibrium, the product gas has ample opportunity to equilibrate as it passes through the thick Ni-YSZ anode. While Fig. 12 also correctly predicts that coking is suppressed at high enough *J*, a quantitative comparison shows that the overall χ values in our experiments were only ≈ 0.05. While this value is too low to explain the lack of coking, it should be noted that cell reaction products are concentrated within the anode, which may lead to a high "local" χ value. Simulations of the fuel-gas composition within the anode are required to obtain a better understanding of direct-methane operation.

These results indicate that in a SOFC operating on humidified CH_4, a number of species are present within the Ni-YSZ anode including C, H_2, H_2O, CO, and CO_2. From the present results, it is still not clear what are the key kinetic pathways for anode operation. The possible reaction pathways on the anode side are as follows:

$$CH_4 = C + 2H_2 \quad (4)$$

$$CH_4 + O^{2-} = CO + 2H_2 + 2e^{2-} \quad (5)$$

$$CH_4 + 4O^{2-} = CO_2 + 2H_2O + 8e^{-} \quad (6)$$

$$CH_4 + H_2O = CO + 3H_2 \quad (7)$$

$$C + O^{2-} = CO + 2e^{-} \quad (8)$$

$$C + 2O^{2-} = CO_2 + 4e^{-} \quad (9)$$

$$CO + O^{2-} = CO_2 + 2e^{-} \quad (10)$$

$$CO + H_2O = CO_2 + H_2 \quad (11)$$

$$H_2 + O^{2-} = H_2O + 2e^{-} \quad (12)$$

Matruzaki et. al.[6] studied the electrochemical oxidation of H_2 and CO in a H_2-H_2O-CO-CO_2 system at the interface of a Ni-YSZ cermet electrode and YSZ electrolyte and showed that at high temperatures, the reaction rate of (12) is much faster than (10) and the shift reaction (11) is

faster than the electrode reaction. There are also several other reports[8,9,10] showing that the oxidation of hydrogen is the main electrode reaction on the Ni-YSZ cermet electrode in a CH_4-H_2O system when S/C is higher than unity. One could argue that eq. 12 is also the primary kinetic pathway for the direct-methane SOFC. In this case with very low S/C ratio, the H_2 generated via eq. 7 is limited due to the small amount of H_2O. However, H_2 is also generated via eq. 4 and, at higher *J*, by reformation via reaction products (e.g. reaction 7), as indicated by Figs. 11 and 12. According to Fig. 12, H_2 is the main gas-phase product at equilibrium, such that the diffusion limiting current given by eq. 3 should be similar to that for pure H_2 fuel – this agrees with the results in Figs. 1a and 1b which show similar limiting currents for H_2 and CH_4. One problem with this interpretation is that it cannot explain the high OCV values observed for methane (Fig. 4). Indeed, the calculated equilibrium OCV shown in Fig. 4 includes solid C (Fig. 12) on the anode; carbon oxidation (e.g. reaction 8) must be involved to some extent in order to produce this high OCV.

Detailed modeling of the diffusional processes and chemical reactions within the Ni-YSZ anode are required to fully understand this problem

5. Extended cell testing

Cell Stability and Coking Effects – Ni-YSZ

We have mapped out the stability region (versus temperature and current density) for anode-supported SOFC operation on methane. Figure 13 shows results taken at 700, 750, and 800^{o}C. In these tests, the cell was initially operated with hydrogen for ≈ 40 h to reduce the anode and fully stabilize the cell performance. After that the cells were switched to methane and operated at high *J* (near the maximum power point). *J* was reduced in steps, and the cell operated for 3-4 h in each step, long enough to observe whether coking-induced degradation

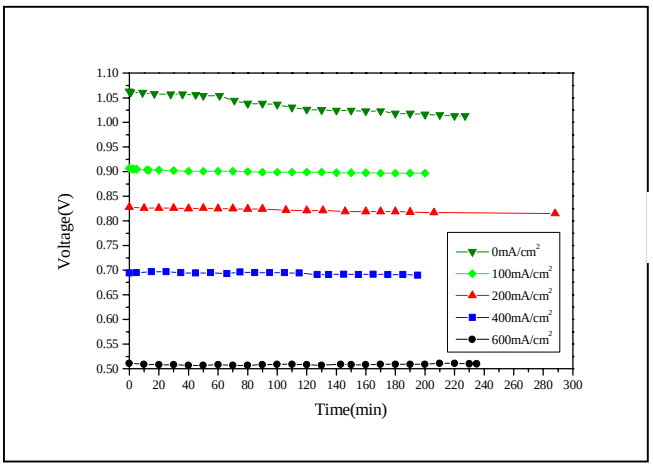

(a) 700°C

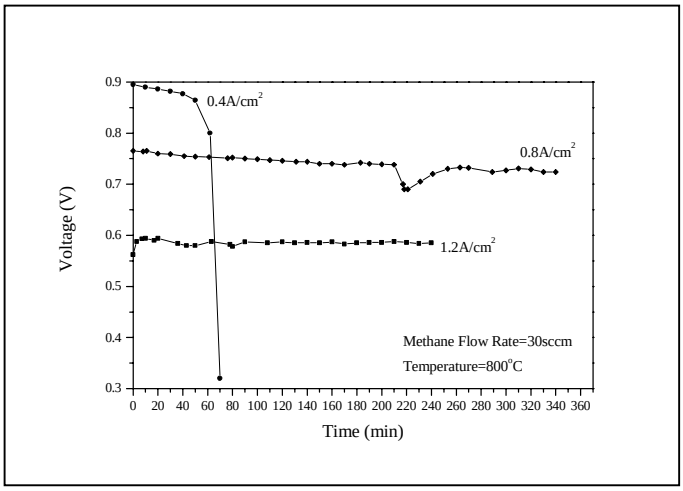

(b) 750°C

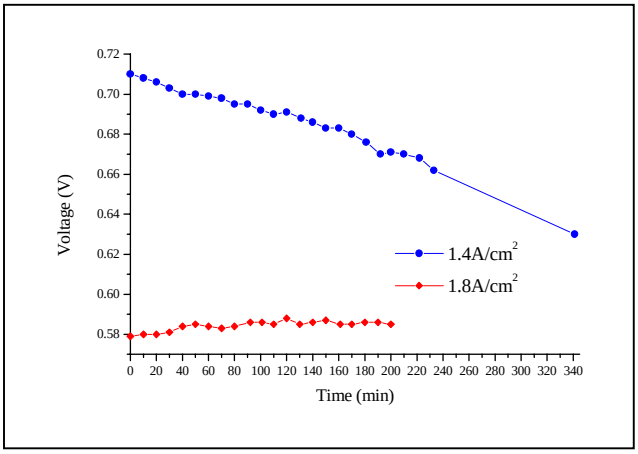

(c) 800°C

Figure 13. Results of SOFC tests in humidified hydrogen at 700 (a), 750 (b), and 800°C (c). The cells were operated at different *J* values for 3-4 h in each step, starting at high *J* and reducing *J* in steps.

occurred. As shown in Fig. 13a, 700C, stability in methane was excellent as long as a minimum cell current density J = 0.1 A/cm^2 is maintained. At J = 0, on the other hand, the voltage degraded gradually over several hours. The results were similar at 750 (Fig. 13b) and 800^{o}C (Fig. 13c), but increasingly large critical current values, $0.8 < J_c^{750} < 1.2$ A/cm^2, $1.4 < J_c^{800} < 1.8$ A/cm^2, respectively, were needed to maintain stable operation. This is reasonable given that the rate of methane cracking increases rapidly with increasing T above ≈700C, and assuming that the oxygen ion flux was needed to prevent coking.[11] A few initial experiments varying methane flow rate and anode thickness/porosity showed that these factors have relatively weak effects on the critical J value for maintaining stable operation. In addition, a few longer tests were carried out for longer times to help assure that coking was not occurring beyond the 3-4h time frames shown in Fig. 13. As shown in Fig. 14, a cell operated in methane was stable during a 100 h test.

Initial attempts have been made to examine the effect of methane concentration on stability. This is relevant to understanding SOFC operation in partially-reformed hydrocarbon fuels, where there will be significant amounts of methane present. In these initial experiments, the effect of methane concentration alone was examined (i.e. without introducing any other reforming species) by using a 50% methane – 50% Ar mixture. The SOFC stability results at 800^{o}C results are shown in Figure 15. The cell was fairly stable except for J = 0, a remarkable improvement from the 800^{o}C result shown in Fig. 13c. This result indicates a surprisingly strong dependence on methane concentration. Further work is needed to fully characterize and understand this effect.

Visual observation and SEM-EDX measurements after cell tests showed coke on the anodes only in cases where performance degraded. Furthermore, for heavy coking, clear degradation of the anode structure was visible in the SEM, as the coke built up in the anode

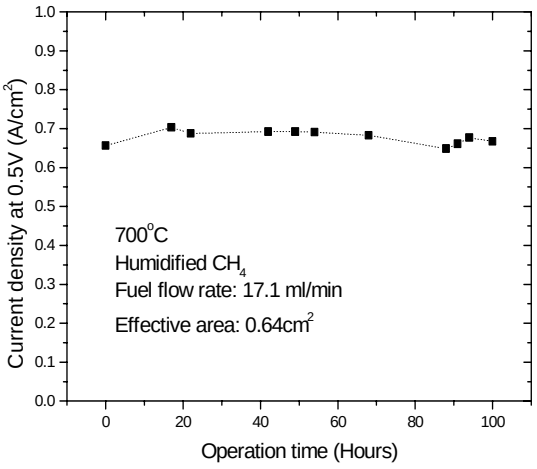

Figure 14. Results of an extended SOFC test at 0.5V in humidified hydrogen at 700^{o}C.

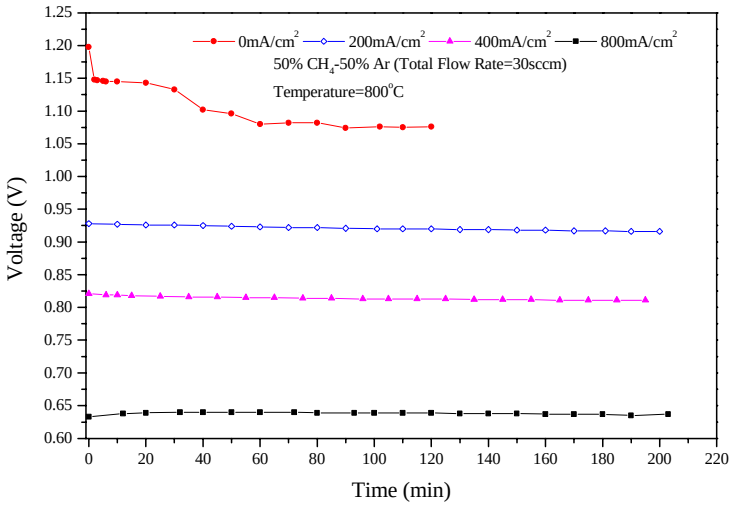

Figure 15. Results of SOFC tests in humidified hydrogen at 800°C. The cell was operated at different *J* values for 3-4 h in each step, starting at high *J* and reducing *J* in steps.

causing volume expansion. Figure 16 shows an example of the surface structure of an anode after degradation. The SOFCs finally fail when the coking causes sufficient anode expansion to crack the electrolyte. These results clearly link the degradation to coking.

SEM-EDX measurements also provided insight into the coking process in the anodes. For this measurement, a SOFC was operated in humidified methane at 700°C for several hours and then was cooled rapidly in Ar. Figure 17 shows that a small EDX carbon signal was present in the anode, and that it varied as a function of depth through the anode. The carbon content increased from the electrolyte interface to the free surface. This variation can be understood based on a simple model of gas composition versus depth during direct-methane operation, shown schematically in Fig. 18. It is well known that mass transport through the anode produces substantial partial pressure gradients, especially at high current densities.[5] Thus, the methane partial pressure decreases from the free surface to the electrolyte, whereas the product partial pressures follow the reverse trend. Note that the simplified model shown in Fig. 18 does not include reforming reactions that will occur within the anode. These will consume CH_4, H_2O, and CO_2, such that the concentration gradients shown will be increased. In any case, it is clear from Fig. 18 that the conditions for coking are most favorable near the free surface, in good agreement with the results in Fig. 17. Note that the enhanced product concentrations and reduced methane concentration in the anode helps explain the lack of coking during SOFC operation.

Redox Cycling – Ceramic Anodes

A well-known problem with Ni-YSZ anodes is the degradation that occurs upon redox cycling.[12] Ceramic-based anodes provide an opportunity to avoid this problem because there is little volume expansion or contraction upon reduction and oxidation. To test this hypothesis, we carried out redox cycling experiments on the GDC-electrolyte cells with LSCV-GDC-Ni anodes.

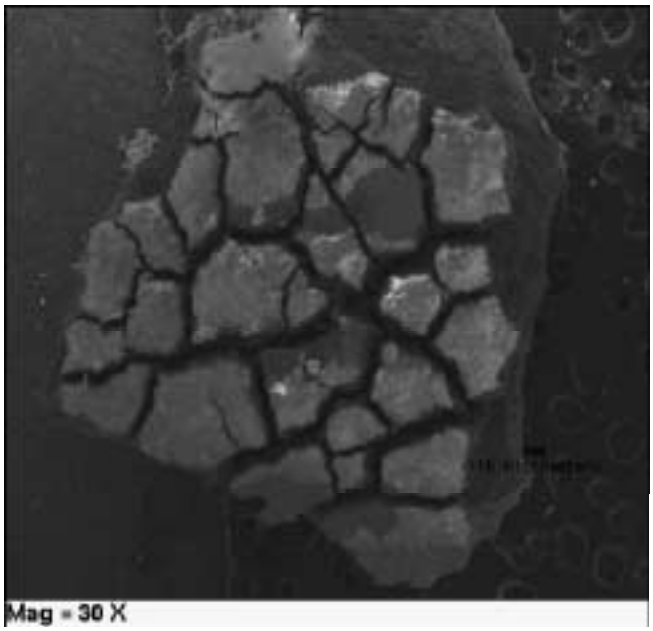

Figure 16. Optical micrograph showing an example of severe coking of an anode surface, after cell operation under conditions leading to performance degradation. There is clear cracking of the anode (lighter areas) by the introduction of carbon (darker areas).

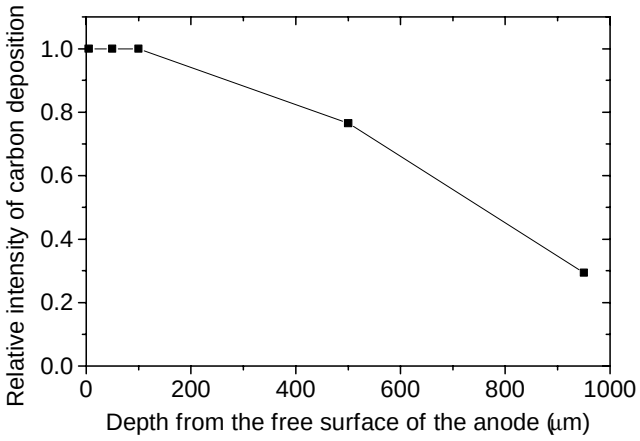

Figure 17. SEM/EDX measurement of the C signal versus depth in an anode after cell testing in humidified methane at 700C.

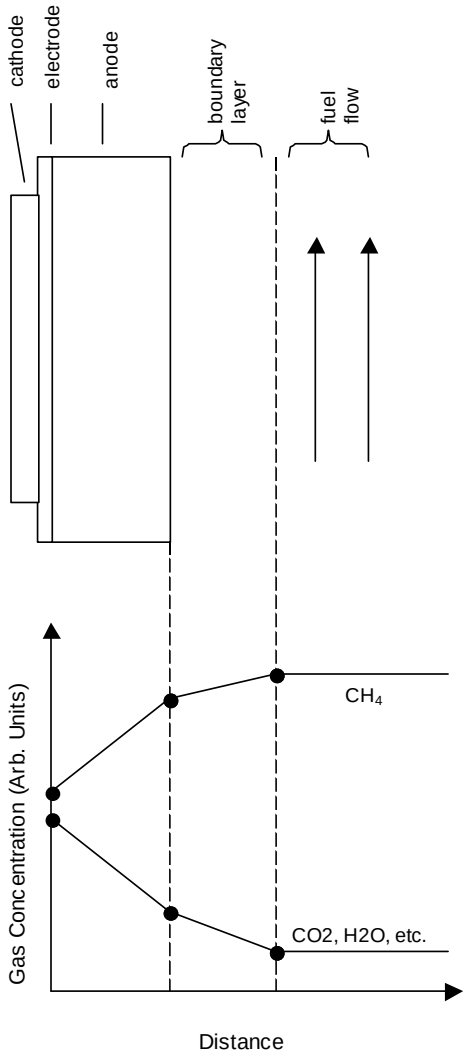

Figure 18. Simplified schematic illustration of how reactant and product gas concentrations are expected to vary with position during SOFC operation.

Figure 19 shows the result for hydrogen-air (a) and propane-air (b) cycling. In the hydrogen-air case, the cell was maintained at a constant voltage of 0.5V. In the propane-air case, the cell maintained at a constant current of 200 mA/cm^2. The cell was operated for ≈ 30 min in fuel, then the fuel flow was stopped and air allowed to enter to fuel compartment. The cell voltage and current rapidly dropped to zero. After ≈ 30 min, the fuel flow was re-started, whereupon the cell voltage and current rapidly returned to close to their original values. This cycle was repeated several times with similar results. Note that the transients at the beginning of fuel flow may be related to the time required to fully flush any air from the fuel lines. A total of 30 redox cycles were carried out during this cell test with no evidence of cell degradation. These results strongly indicated that ceramic-based anodes avoid problems with redox cycling.

6. Sulfur Poisoning

Ni-YSZ anode-supported cell tests were carried out using H_2 fuel with 10 ppm H_2S. Figure 20 shows the results at 800°C (a) and 700°C (b) for the following cases: in dry pure H_2 before exposure to sulfur, during stable operation in H_2-10ppmH_2S, and after the returning to pure H_2 and allowing the cell to reach steady state performance. The effect of H_2S was minor at 700°C, but there was a substantial degradation at 800°C. This result is rather surprising based on prior results for 750 – 1000°C suggesting that sulfur poisoning is exacerbated as the temperature is reduced.[13] More work is needed to verify this result.

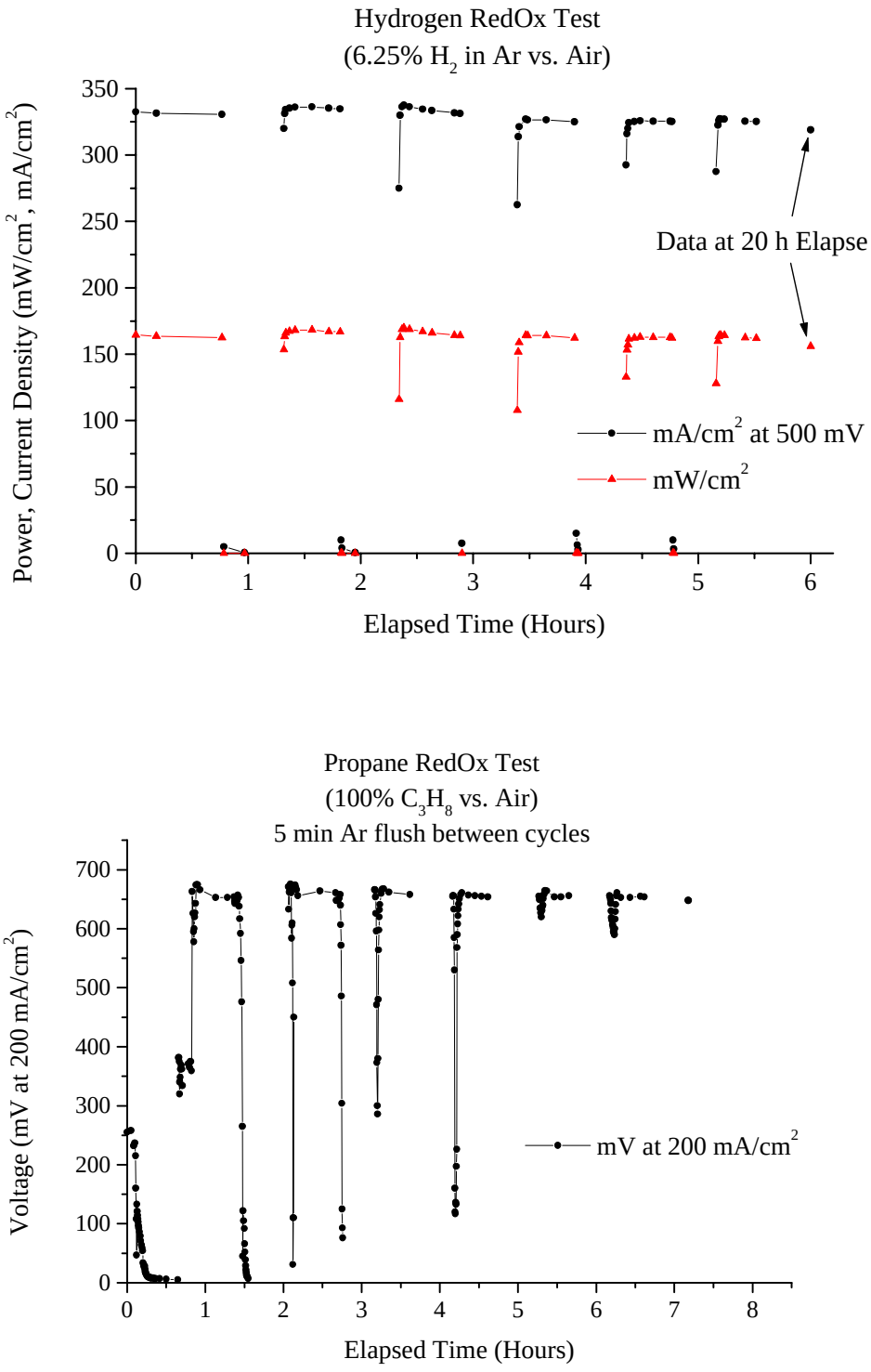

Figure 19. Redox cycling result for hydrogen-air (a) and propane-air (b) cycling.

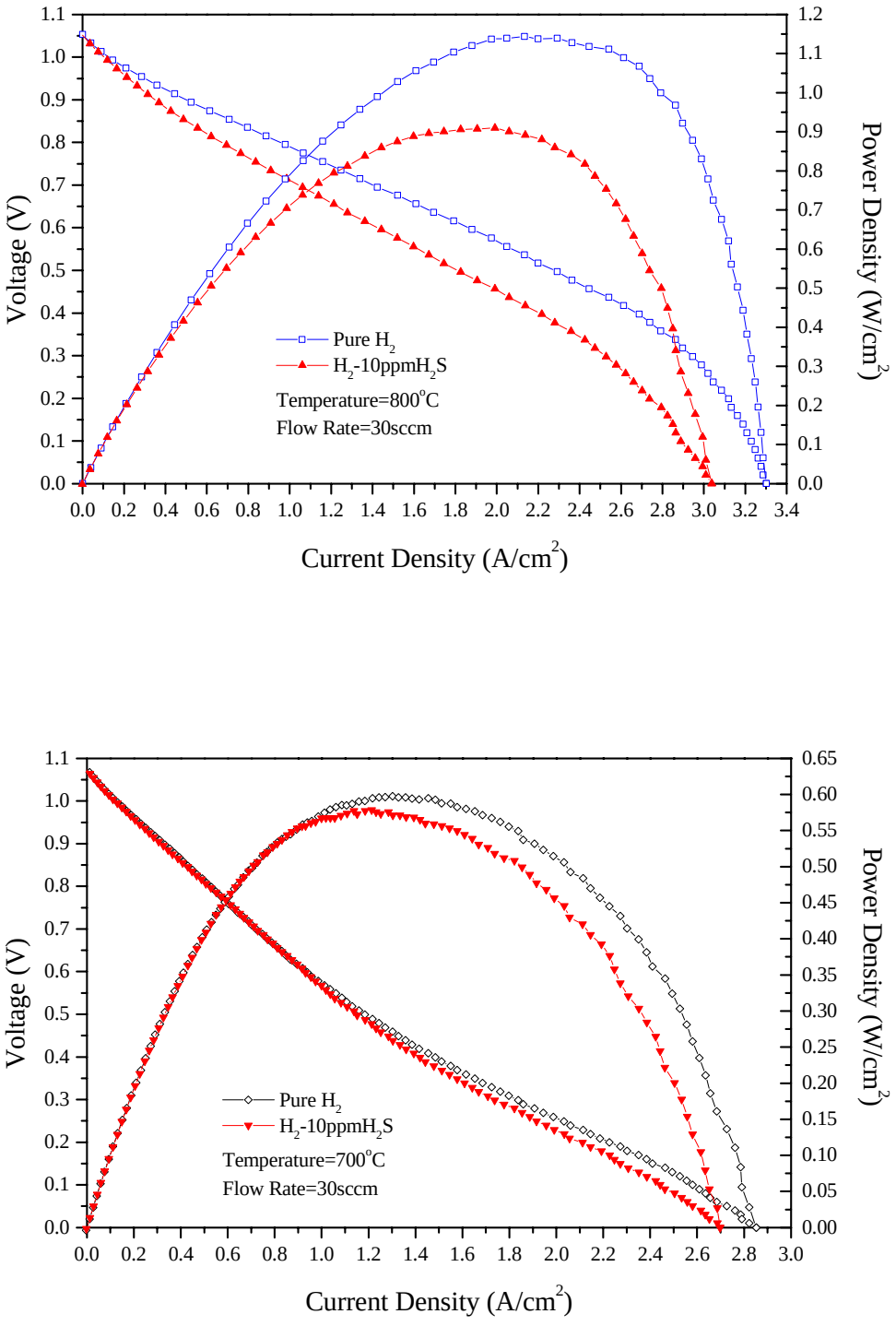

Fig. 20. Cell performance in dry pure H_2 and H_2-10ppmH_2S at 800°C (a) and 700°C (b).

7. Ceramic Anode Supported SOFCs

SOFCs with YSZ thin electrolyte layers prepared by centrifugal coating onto $Sr_{0.55}La_{0.3}TiO_3$-GDC-NiO anode supports have been successfully prepared. The coated supports were co-sintered at 1400^{o}C for 6h. Figure 21 shows a cross-sectional SEM micrograph of the resulting structure. The ≈ 15 μm thick electrolyte layer appears to be quite dense. The support shows considerable porosity on a large scale due to the addition of a filler material (starch) during preparation. Some curvature was observed in the resulting pellets; this can be solved by improving the ceramic processing procedures. Initial cell testing is under way.

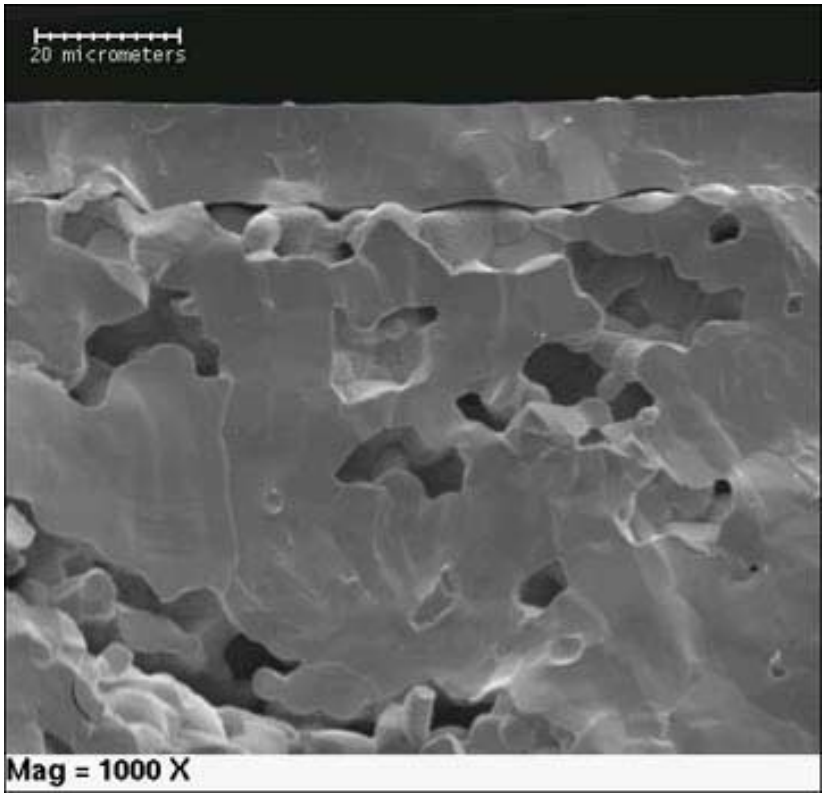

Figure 21. Cross-sectional SEM micrograph of a YSZ thin electrolyte layer prepared by centrifugal coating onto a $Sr_{0.55}La_{0.3}TiO_3$-GDC-NiO anode support, after co-sintering.

V. Conclusions

A broad study of the operation of Ni-YSZ anode supported SOFCs directly on methane has been carried out. While many experiments remain to be done, the results are beginning to provide a clearer picture of how these cells operate. Furthermore, they have made it clear that there is a range of conditions where SOFCs can be successfully and stably operated on methane. In addition, studies of ceramic-based anodes have confirmed key advantages of these materials, including ability to work with a range of hydrocarbon fuels and good performance under redox cycling. Nonetheless, considerable work remains to be done to understand the operation of these anodes, and to improve power densities to viable levels. The following are the main conclusions of this Phase I study.

(1) Improvements in cell fabrication have allowed improvements in SOFC performance with methane fuel. Power densities as high as 0.45 W/cm^2 at 700^{o}C and 1.1 W/cm^2 at 800^{o}C have been achieved. It is clear that further improvements are possible.

(2) Open circuit voltages approaching 1.2 V are one of the reasons for the good performance in methane. Good fits to the OCV data for various fuel compositions were obtained based on equilibrium calculations in most cases. One exception was for CH_4-CO_2-H_2O mixtures at temperatures below 750^{o}C, where the OCV value suggested that the fuel had not equilibrated.

(3) EIS measurements were carried out primarily on SOFCs, because attempts to do measurements on symmetric anode samples did not yield reasonable results. The SOFC results showed that the cathode polarization dominated only at very low current density. With increasing current, the cathode polarization decreased rapidly to a saturation value, whereas the anode polarization increased continuously with

increasing current. The anode polarization was substantially larger for methane than for hydrogen. These results indicate that gas diffusion in the anode support played an important role in determining cell performance; this suggests that, in general, SOFC performance will be strongly dependent on anode parameters including thickness, porosity, and tortuosity. For ceramic-based anodes, the anode polarization was substantially larger in propane than for hydrogen.

(4) Mass spectrometer measurements showed that the expected reaction products – H_2, H_2O, CO, and CO_2 – all increased with increasing cell current density. The dominant products at 800^oC were H_2 and CO, in agreement with thermodynamic predictions. However, the thermodynamic predictions could not directly explain the lack of coking during direct methane operation.

(5) The nature of the key anode reaction(s) remains unclear at this stage. While there is good reason to think that substantial hydrogen is produced within the Ni-YSZ anode, the OCV values observed experimentally cannot be explained by a hydrogen oxidation reaction. More work, particularly detailed modeling of diffusion and reaction processes within the anode, is needed.

(6) We have mapped out the stability region for direct methane operation. The key features are as follows. At lower temperatures, ≤700^oC, stable operation without coking occurs over a wide range of current densities. At higher temperatures, on the other hand, increasingly large currents are required to avoid coking and cell failure. Fuel gases containing lesser amounts of methane appear to have a much wider stability range. Thus, direct-methane SOFC stacks would be best operated at lower

temperatures. Even a minimal partial reforming of the methane, prior to introduction to the stack, will substantially improve stability.

(7) Degradation of cell performance was observed for H_2S-contamined H_2 fuel at 800^oC, but surprisingly the degradation was negligible at 700^oC. Further work is needed to explore these effects.

(8) Further experiments have been carried out on ceramic-based anodes. Cells tests with these anodes have shown good fuel flexibility, including hydrogen, methane, ethane, propane, and butane. Excellent cell stability, particularly in redox cycling with hydrogen-air and propane-air, has been demonstrated. Increased power densities are required, however.

References

[1] J. Liu, B. Madsen, and S.A. Barnett, Electrochem. Solid State Letters 5, A122 (2002).

[2] S. Park, R.J. Gorte, and J.M. Vohs, Applied Catalysis A **200,** 55-61 (2000).

[3] J. Liu and S. A. Barnett, J. Am. Ceram. Soc., 85, 3096 (2002).

[4] S. B. Adler, J. A. Lane and B. C. H. Steele, J. Electrochem. Soc., 143, No. 11, (1996) 3554-3564.

[5] J.W. Kim, A.V. Virkar, K.Z. Fung, K. Mehta, and S.C. Singhal, J. Electrochem. Soc. 146, 69 (1999).

[6] Y. Matsuzaki and I. Yasuda, J. Electrochemical Society, 147, 1630 (2000).

[7] A. Abudula, M. Ihara, H. Komiyama, K. Ynada, Solid State Ionics, 86-88, 1203 (1996).

[8] T. Kawada, I. Anzai, N. Sakai, H. Yokokawa, and M. Fokiys, in High Temperature Electrode Materials and Characterization, D. D. Macdonald and A. C. Khandkar, Editors, PV 96-6, p. 165, The Electrochemical Society Proceedings Series, Pennington, NJ (1991).

[9] S. Onuma, A. Kaimai, K. Kawamura, Y. Nigara, T. Kawada, J. Mizusaki, H. Inaba, and H. Tagawa, J. Electrochem. Soc. 145, 3117 (1998).

[10] S. Onuma, A. Kaimai, K. Kawamura, Y. Nigara, T. Kawada, J. Mizusaki, H. Inaba, and H. Tagawa, J. Electrochem. Soc., 145, 920 (1998).

[11] C.M. Finnerty, N.J. Coe, R.H. Cunningham, and R.M. Ormerod, Catalysis Today 46 (1998) 137.

[12] Reitveld, G., Nammensma, P., Ouweltjes, J.P., In *Proc. 7th Int. Symp. On Solid Oxide Fuel Cells* (Yokokawa, H. and Singhal, S.C., Editors), Electrochem. Soc., p125 (2001).

[13] Y. Matsuzaki and I. Yasuda, In *Proc. 7th Int. Symp. On Solid Oxide Fuel Cells* (Yokokawa, H. and Singhal, S.C., Editors), Electrochem. Soc., p 769 (2001).